Tribology International 169 (2022) 107488

Contents lists available at ScienceDirect

Tribology International

journal homepage: www.elsevier.com/locate/triboint

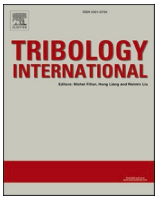

Lifetime assessment of porous journal bearings using joint time-frequency analysis of real-time sensor data

J. Prost [a], G. Boidi [a], M. Varga [a], G. Vorlaufer [a], S.J. Eder [a,b,*]

[a] AC2T research GmbH, Viktor-Kaplan-Straße 2/C, 2700 Wiener Neustadt, Austria
[b] Institute of Engineering Design and Product Development, TU Wien, Lehárgasse 6 — Objekt 7, 1060 Vienna, Austria

ARTICLE INFO

Keywords:
Porous journal bearing
Mixed lubrication
Failure
Numerical analysis

ABSTRACT

In this work, we employed a custom-built tribometer that allows simultaneous testing of five porous journal bearing systems to perform lifetime tests on combinations of bearing materials and lubricants at various temperatures. Test parameters and contact conditions were tailored to promote mixed/boundary lubrication and accelerated wear tests. Failure and wear data were evaluated ex-post, leading to survival probability curves based on Weibull fitting that allow quantitative ranking of bearing life as well as qualitative assessment of the failure behavior. Friction torque and accelerometer data were recorded either continuously or at regular time intervals, with the potential for on-the-fly evaluation. Using joint time-frequency analysis, we produced spectograms of the accelerometer data, which can characterize the state of operation and allow a clear disambiguation of the running-in phase, steady-state behavior, and critical operation before failure.

1. Introduction

Porous journal bearings (PJBs) are inexpensive machine elements that are produced using powder metallurgical methods [1], where the resultant pores act as oil reservoirs to maintain a continuous lubricant supply between shaft and bearing. Due to their self-lubricating behavior [2,3], they operate under hydrodynamic lubrication conditions for most of their service life, as long as the pores are sufficiently filled with lubricant [4]. However, under certain conditions such as start/stop operation [5,6] or after long and severe use (e.g., high loads and temperatures), the lubrication regime may shift towards mixed or boundary lubrication, depending on how much oil is left in the pores.

Although PJBs have been studied since the 1950s [2,3,7], some research topics remain open, such as surface texturing [8], novel lubricants [9,10], the phenomenon of cold squealing [11], or the assessment of failure probability over time. PJBs are designed for service lives upwards of 10,000 h [12], so standard experimental tests to predict the lifetime are cumbersome and costly, as a single test may go on for several weeks or even months. The authors have recently developed a heatable test rig allowing simultaneous testing of five bearings. This rig can be utilized for either increasing the data acquisition bandwidth, for obtaining a reliable statistical analysis by testing identical bearing/lubricant combinations in parallel [13], or for speeding up test trials at elevated temperatures [14,15]. In particular, the experimental methodology established by the authors [13–15] was designed to test the PJBs under mixed/boundary lubrication, therefore promoting asperities contact and wear (accelerated tests).

Joint time-frequency analysis (JTFA) is a powerful and versatile tool for the localization of quasi-periodic patterns in time within non-periodic time-series data. The two most common procedures are based on the short-time Fourier transform (STFT) [16] or the wavelet transform [17]. Industry-related applications of JTFA include the evaluation of transient vibrations in rotating machine components [18], fault detection in water pipelines [19], machinery fault diagnosis [20,21], and tool condition monitoring [22,23]. In tribology, JTFA is predominantly applied to acoustic emission signals and used for wear detection and monitoring [24,25], as well as for the automated detection and prediction of failure mechanisms in combination with machine learning approaches [26,27]. Recently, the occurrence of abrasive wear in journal bearings under hydrodynamic lubrication could be linked to speed-dependent vibrations [28,29]. At the authors' institution, JTFA was applied to detect cold-induced noise emissions from PJB using piezo-electric vibration sensors in recent years [11]. JTFA has also proven to be a powerful tool to detect transient dynamic changes in pin-on-disc tribometer experiments [30].

In this work, we have combined several of the test rig's experimental features with JTFA of vibration data obtained from piezo-electric

* Corresponding author at: AC2T research GmbH, Viktor-Kaplan-Straße 2/C, 2700 Wiener Neustadt, Austria.
E-mail address: stefan.j.eder@tuwien.ac.at (S.J. Eder).

https://doi.org/10.1016/j.triboint.2022.107488
Received 29 November 2021; Received in revised form 4 February 2022; Accepted 9 February 2022
Available online 11 February 2022

Nomenclature

PJB	Porous Journal Bearing
MPPS	Methylphenyl-Polysiloxane
PG	Polyglycol
CoF	Coefficient of Friction
RT	Room Temperature
JTFA	Joint Time-Frequency Analysis
HR	High-resolution
FFT	Fast Fourier Transform
PSD	Power Spectral Density
STFT	Short-Time Fourier Transform

accelerometers to study transitions between different operation regimes during run-time. Mixed/boundary lubrication conditions were evaluated in our experimental workflow, since these lubrication regimes are quite complex to simulate, and also to promote accelerated wear tests. We compare the friction and wear performance of four bearing–lubricant combinations (two bearing materials × two lubricant types) and analyze their vibrational behavior during run-in, the steady state, and the critical phase leading up to failure. The vibration analysis focused on identifying the main vibration modes rather than identifying the origin of every vibration signal's frequency component. Finally, we provide survival probability curves of those bearing–lubricant combinations that failed during testing, based on Weibull fits to the time-until-failure.

2. Experimental details

2.1. Test setup and conditions

Tribological tests were performed using a custom-built multiple bearing wear test rig [13]. The test rig, see Fig. 1, was conceived to run simultaneously five identical tribotests for obtaining statistically reliable results in reduced run-times. Each shaft is driven by an electric motor with a frequency converter, allowing continuous speed variations. The load is radially applied on each shaft using a dead weight on a rod (pendulum). The temperature of the bearing can be controlled and increased up to 180°C during the test. The bearing temperature is constantly measured using a thermocouple fixed in a hole in the side of the bearing near the sliding surface. The coefficient of friction (CoF) is calculated using the torque measurements obtained from the electric signal of the frequency converter. Uni-directional piezo-electric accelerometers were attached to the body of the sample holder on three of the five test positions and used for detecting vibrations associated with bearing failure evolution. The accelerometers were positioned to measure the acceleration radially in the same direction as the applied load. A more detailed description of the test rig can be found in previous publications from the authors [13–15].

Motor torque, rotational speed, and temperature signals were continuously acquired at low sampling rate (5 Hz) throughout the experiment. High-resolution (HR) data of the same sensors were recorded during 180 s time windows every hour at an acquisition rate of 2 kHz. Additionally, accelerometer data were acquired within the same time intervals at an acquisition rate of 20 kHz.

The tests ran under a constant specific bearing load (radial load divided by the projected cross-section of the bearing) of 3 MPa (25 kg/245 N load), and the speed varied between + 20 and –20 rpm following a saw-tooth profile with a frequency of 0.1 Hz. Each bearing-material–lubricant combination was tested at room temperature (RT), 100°C, and 160°C. Some tests at 160°C using a specific lubricant were omitted because severe wear already occurred at 100°C, see Section 3.1. A test at a particular bench position was independently stopped and considered a failure of the bearing when the motor torque exceeded a threshold value of 0.8 Nm. The entire test rig was stopped when at least three bearings had failed and failure of the remaining bearings was foreseeable. The test rig was shut down manually after approximately two weeks (11–14 days), if at least four bearings were still operational after that time.

2.2. Bearing materials and lubricants

For this study, custom-fitted PJB of two different materials, bronze and iron-based, were used, see the composition in Table 1. The bearings had an external diameter of 15.6 mm and a length of 11 mm. The bore diameter was fitted by the manufacturer to 8.033 ± 0.01 mm.

Commercially available martensitic stainless steel (X90CrMoV18) shafts were utilized as counter-body and replaced after each test. The samples had a nominal diameter of 8 mm with h6 tolerance (0/−9 μm). The shafts had a surface hardness of minimum 54 HRC and a surface roughness of $Ra \leq 0.3$ μm. The average diametric gap between bearing and shaft was hence 37.5 μm, or 0.47%. The gap height was selected to accelerate the wear tests because of increased asperity contact compared to usual PJB applications. Furthermore, the diametric gap was designed to avoid undesired bearing compression due to thermal expansion of the

Table 1
PJB materials and compositions used for the tribological tests.

Material	Composition	Density (g/cm^3)	Total porosity (%)	Average pore size (μm)
Iron-based	Fe + 2% Cu	5.8	25	5.8
Bronze	pure bronze	7.2	20	3.3

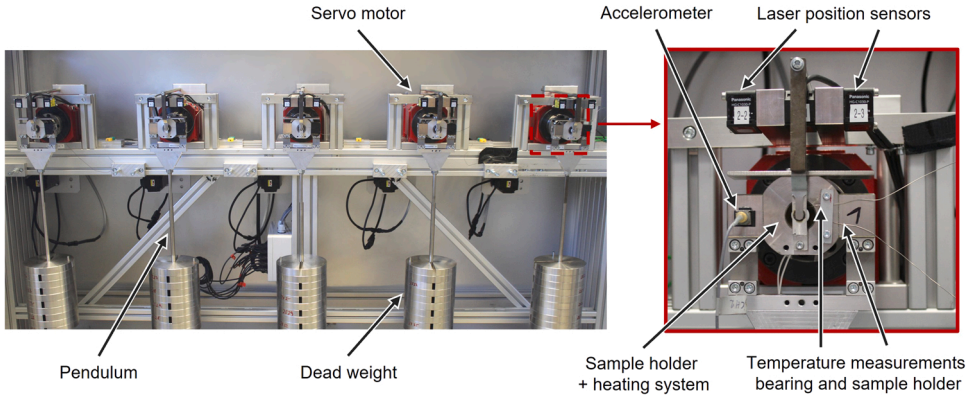

Fig. 1. Overview of the multiple bearing wear test rig.

samples because of the large temperature range in the experimental matrix (maximum thermal expansion ≈ 25 μm at 160°C).

The selected bearing materials had distinct densities and total porosities, see Table 1. The tribological properties of sintered materials strongly depend not only on the total porosity, but also on the porosity characteristics [31–33]. Therefore, principal pore characteristics were optically determined. Pictures from three randomly selected regions of each material were taken and then quantitatively analyzed using the open-source software ImageJ [34]. The pore size distribution and the corresponding pore area fraction (percentage of area occupied by the pores) are shown in Fig. 2. Furthermore, the average pore sizes obtained by optical analysis are listed in Table 1. The iron-based bearings feature a higher volumetric porosity than the bronze-based ones, and the pores are generally larger. For instance, medium-sized pores (between 20 and 60 μm) occupied much more area in the iron-based bearings compared to the bronze PJB material, see Fig. 2.

The bearings were cleaned and then filled with the lubricants listed in Table 2 following a standardized routine detailed in a previous publication [13]. Two commercially available lubricants were used, namely polyglycol (PG) and methylphenyl-polysiloxane (MPPS), featuring a considerable difference in viscosity indices, see Table 2. Note that the viscosity at RT and 160°C was estimated using the Walther equation. The shear rate under test conditions ranged between 10^3 and 10^4 s^{-1}, so shear thinning could be ruled out. The lubricant selection was based on knowledge from previous studies [15] with the intention to test one oil associated with high wear rates under mixed lubrication conditions (MPPS) and one with intermediate performance (PG), so that bearing system failures would occur within reasonable amounts of time. All bearings were impregnated with lubricant to at least 95%.

2.3. Data evaluation

2.3.1. Friction and wear measurement

The presented test rig allows the determination of the friction torque and subsequently the CoF in two different ways. Firstly, the electric current used to power the servo motor is continuously monitored by the acquisition software. The motor torque is proportional to the recorded motor current. The friction torque is then obtained by subtracting the running-idle torque from the measured signal. This method does not

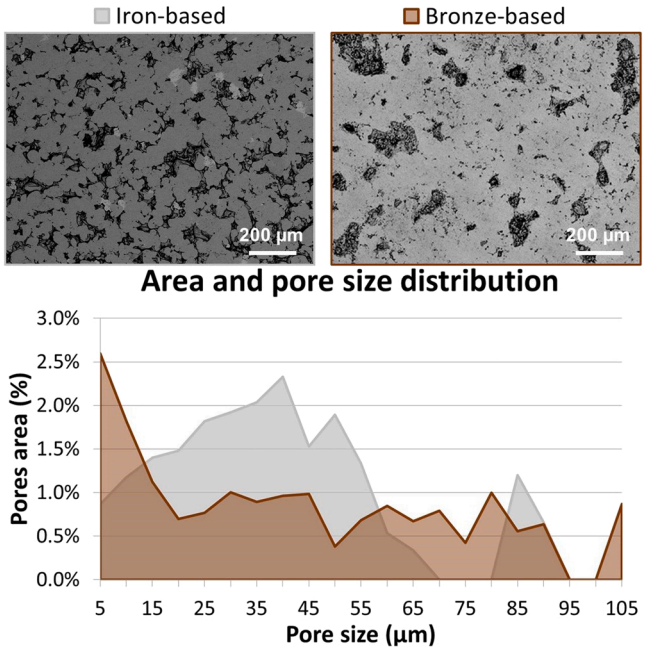

Fig. 2. Comparison of the porosity between iron-based and bronze-based PJB materials.

Table 2
Lubricants used for the tribological tests.

Abbreviation	Lubricant base	Density (g/cm^3)	Viscosity (mPa · s) (RT*/40°C/ 100°C/160°C)	Viscosity index
PG	Polyglycol	1.04	85/46/9/3.6	181
MPPS	Methylphenyl-Polysiloxane	0.95	174/130/52/ 27	413

*RT was considered 25°C for evaluating the viscosity

provide high-accuracy results. However, it is suitable for long-term tests at low rotational speeds and low acquisition rates, as is the case in the current study. The second, more precise method uses the signals from three laser position sensors to calculate the friction torque and is described in more detail elsewhere [13]. However, this method is difficult to implement in an industrial setting because it requires additional instrumentation and accessibility of the tribosystem. Therefore, in this work, the CoF (μ) was simply calculated as the ratio of the friction torque M_R, obtained from the recorded motor torque that is readily available in modern drives, and the product of the normal load P and the radius of the shaft r, see e.g., [35,36].

$$\mu = \frac{M_R}{P \cdot r} \tag{1}$$

In order to obtain comparable CoF values for each test and to minimize overall noise, especially spikes at rotational speeds close to zero, only values at the maximum rotational speed $\omega_{max} = \pm 20$ rpm were considered for evaluation. This yields one "envelope curve" for clockwise and one for counter-clockwise rotation, respectively, which are almost identical except for their sign. The CoF values presented in this paper were obtained by averaging the two curves.

Diametric wear of the bearings was measured using a Schwenk OSIMESS two-point measuring instrument for inner diameters of bore holes between 1 and 40 mm [37]. The inner diameter of each bearing was measured before and after the test at three positions: front, center, and rear. Wear was calculated by averaging over the differences between the two measurements at each position.

2.3.2. Accelerometer data

Transient friction-induced vibrations were recorded by a piezoelectric accelerometer. The eigenfrequencies of the pendulum were numerically calculated to discern these values from the broad frequency range obtained through the stochastic interactions of rough surfaces during the tribological test. In order to calculate the characteristic frequency spectra of the vibrations, JTFA was used.

For JTFA, the measured signal $x(t)$ is multiplied by a sliding window function $w(t-\tau)$, and the STFT $X(f, \tau)$ at a given frequency f and a given point in time τ is calculated [16,38],

$$X(f,\tau) = \int_{-\infty}^{\infty} x(t) w(t-\tau) e^{-j2\pi ft}\, dt \quad , \tag{2}$$

with j being the imaginary unit, $j^2 = -1$. For the present work, a Hann window of duration T was used as sliding window function [39]:

$$w(\tau) = \begin{Bmatrix} 0.5 \cdot \left(1 + \cos\frac{2\pi\tau}{T}\right) & \text{if} |\tau| \le \frac{T}{2} \\ 0 & \text{otherwise} \end{Bmatrix} \quad . \tag{3}$$

The squared amplitude of the STFT is known as the Power Spectral Density (PSD) of $x(t)$:

$$PSD = |X(f,\tau)|^2 \quad . \tag{4}$$

In this paper, the PSD is given as a non-dimensionalized quantity, expressed by the logarithmic decibel scale:

$$PSD(\mathrm{dB}) = 10\cdot\log\left|\frac{X(f,\tau)}{X_0}\right|^2 = 20\cdot\log\left|\frac{X(f,\tau)}{X_0}\right| \quad , \tag{5}$$

with $X_0 = 1\ g$, as the output of the accelerometer is given in multiples of $g \approx 9.81\ \mathrm{m/s^2}$.

For visualization, the power spectra of individual windows are stacked along the x (time) axis, and its absolute value is color-coded, yielding a 2D spectrogram of the evolution of the measured vibration frequencies.

3. Results and discussion

3.1. Friction and wear results

3.1.1. Friction curves

Fig. 3 gives an overview of the friction curves obtained for the individual material–lubricant combinations and temperature steps. Bearings lubricated with MPPS exhibited significantly poorer performance compared to PG-lubricated bearings. At RT, MPPS with the iron-based PJB material was the only material combination that exhibited early failure with running times considerably below 200 hours. At 100°C, wear and temperature increase were so severe that failure occurred after an average running time of only 2.5 hours. Therefore, it was decided not to carry out tests with the MPPS lubricant at 160°C. MPPS performed better with the bronze PJB material, with only one early failure at RT after approximately 50 h. At 100°C, four of the five bearings were affected by early failure, albeit running at a slightly lower CoF for the first $\simeq$ 5 hours, and the test rig was stopped after 163 hours.

In contrast, all of the PG-lubricated bearings, independent of the bearing material, were still operational at RT and 100°C when the long-term test was stopped after approximately two weeks. Bronze bearings were running stably throughout the tests, with occasional transient increases of the CoF. It has to be noted that at 100°C the variance between the curves increased after about 230 h, possibly indicating impending failure. For the iron-based bearings with the PG lubricant, a more pronounced run-in behavior was found compared to the other material combinations. This applies especially to the tests carried out at RT, where all bearings stabilized after about 50 h at an average low CoF of 0.06. In contrast, at 160°C, early failure occurred in both PJB materials. For the iron-based bearings, the test rig was stopped after 138 h with three bearings failed and the other two close to failure, running at a high CoF. In these tests, an especially pronounced run-in behavior was observed. Recorded friction torque signals (see Fig. 4) exhibited a higher amplitude in the beginning with a steep decrease after about 10–15 h. This correlates well with outbursts in the accelerometer signals, observed at the turning points of the rotation direction. The increase of the CoF towards the end of the test was also accompanied by outbursts in the accelerometer signal, indicating deterioration of the lubrication condition. These findings will be discussed in more detail in section 3.2. In contrast, only three bronze bearings failed early, preceded by a much slower increase of the CoF.

3.1.2. Statistical analysis

Box plots of CoF and wear results for all material, temperature, and lubricant combinations are shown in Fig. 5. For each test, the middle 50% of each dataset were considered, describing the behavior of the system during stable operation. Colored lines indicate the median of five tests. Boxes extend between the first and third quartiles. Whiskers extend between minimum and maximum, points differing by more than 1.5 times the interquartile range from the median are marked as crosses.

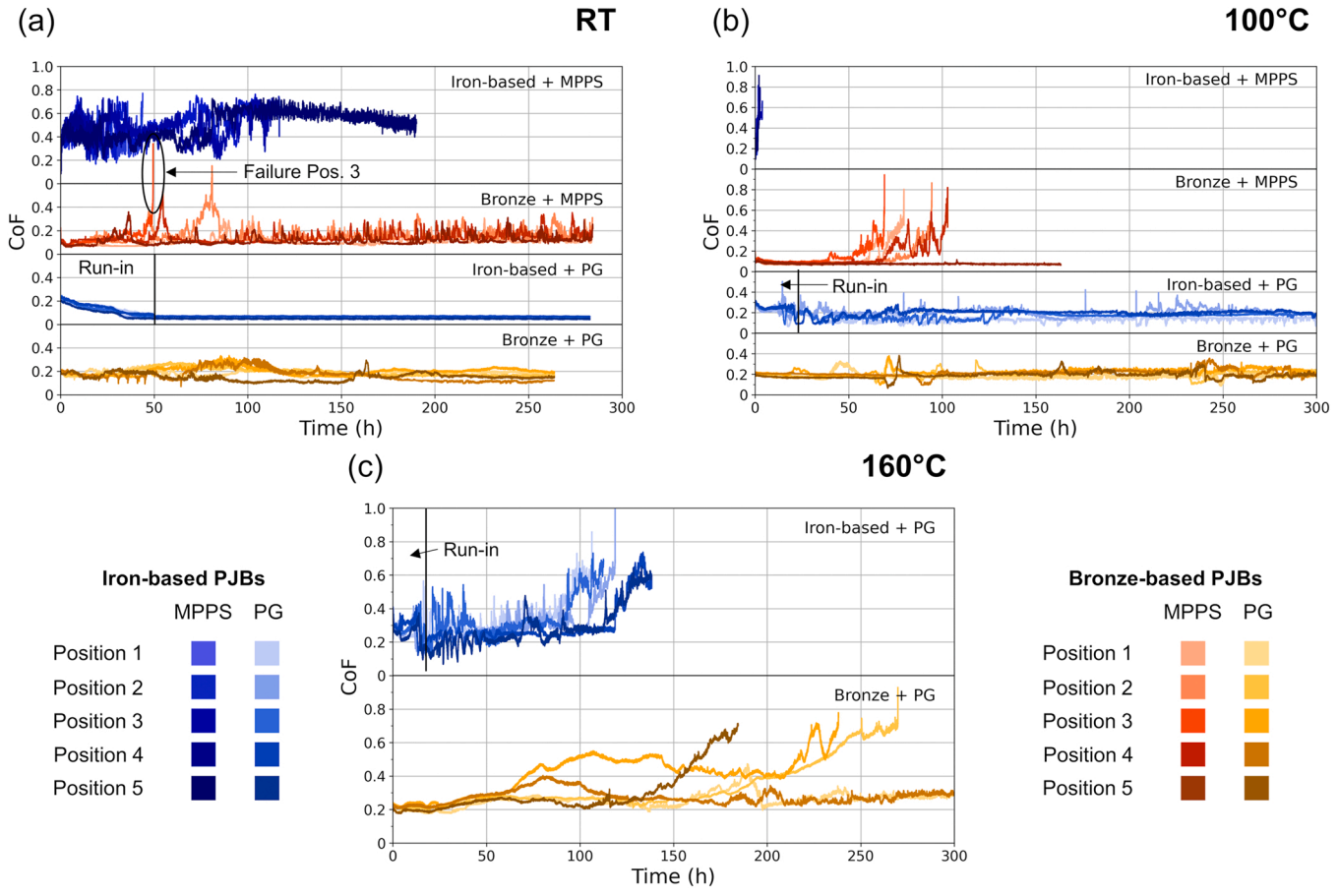

Fig. 3. Friction curves of the various material–lubricant pairings at (a) RT, (b) 100°C and (c) 160°C.

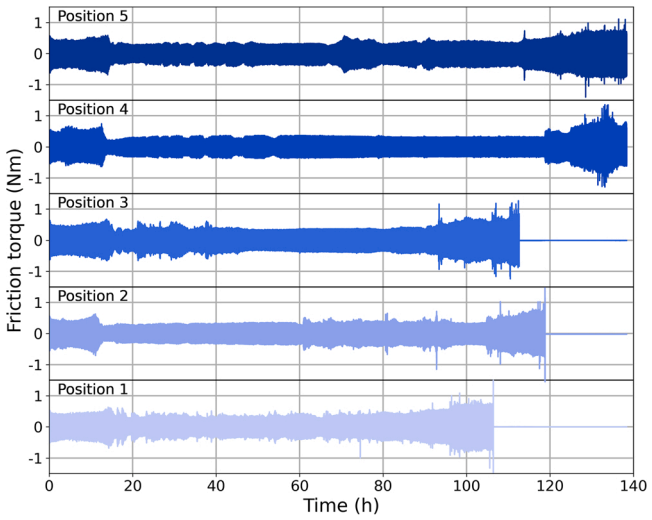

Fig. 4. Recorded friction torque signals for each test position for the material combination iron-based PJBs and PG lubricant at 160˚C, showing clear run-in behavior.

The wear rate, i.e., measured diametric wear divided by the total sliding distance, was used, since bearing lifetime was highly variable, between and even within testing conditions (material, lubricant, temperature).

For iron-based bearings, both CoF and wear were significantly lower using PG than with the MPPS lubricant. This behavior is particularly evident at RT. The use of PG oil led to a strong temperature dependence in combination with the iron-based PJB material, increasing the CoF from 0.07 at RT to 0.18 at 100˚C and 0.27 at 160˚C. A similar, but less pronounced temperature-dependent CoF increase was also found for the bronze bearings with the PG lubricant. An explanation for this increase may be that the increase of temperature reduces the oil viscosity, promoting more asperity contacts and consequently higher friction between the mated surfaces. The PG oil yielded significantly lower wear than MPPS for all bearing materials and temperatures. This difference is particularly pronounced for iron bearings, where wear using the MPPS lubricant was larger by two orders of magnitude compared to PG. Although MPPS yielded a lower CoF in combination with bronze bearings, operation was considerably less stable, and four of the five bearings failed within a time interval of approximately 100 h at 100˚C. In general, bronze bearings exhibited significantly less wear compared to the iron-based ones at all temperatures.

Fig. 6 shows a scatter plot of the wear in dependence of the observed CoF for all four material–lubricant combinations. It can be seen that bronze and iron-based PJB material systems exhibit distinct behavior. While wear remained constantly low for the bronze bearings, a significant wear increase with rising CoF was observed for the iron-based bearings. Furthermore, the two lubricants are clearly separated for both PJB materials, with significantly increased CoF and wear for MPPS in combination with iron-based bearings. By contrast, for bronze bearings, MPPS yielded a lower CoF than PG. Note that the wear of bronze bearings was consistently lower than that of the iron-based bearings, in many cases falling below 10 μm. Six iron-based bearings exhibited critical wear ($>$ 250 μm), causing a significant alteration of the contact geometry. This behavior was mainly observed for iron-based bearings with the MPPS oil, where the lubricant was not able to prevent contact between asperities, thus leading to an increased CoF ($>$ 0.3) and increased wear.

The generally poorer tribological performance of iron-based bearings could be attributed to their larger porosity and pore dimensions compared to the bronze bearings, see Table 1 and Fig. 2. Pore size, quantity, and distribution have a strong impact on the load surface support capacity, as experimentally and numerically studied in [40,41]. Although large pores can act as secondary lubrication sources, they also decrease the surface load support capacity. The larger porosity and pore size of the iron-based PJB material can therefore explain the increased wear rate compared to the bronze samples. Many iron-based samples underwent increased wear, most likely because the surface pores collapsed under severe conditions, promoting greater plastic deformation than bronze samples with fewer and smaller pores [40,41].

3.2. Accelerometer data

JTFA proved to be a powerful tool to distinguish between normal and

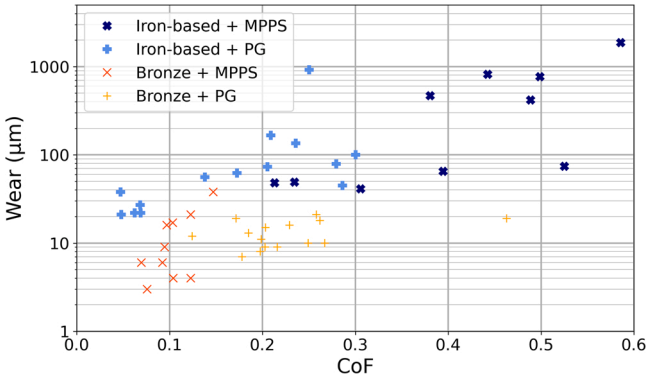

Fig. 6. Average wear in dependence of the measured coefficient of friction (CoF). Iron-based and bronze PJB are clearly separated.

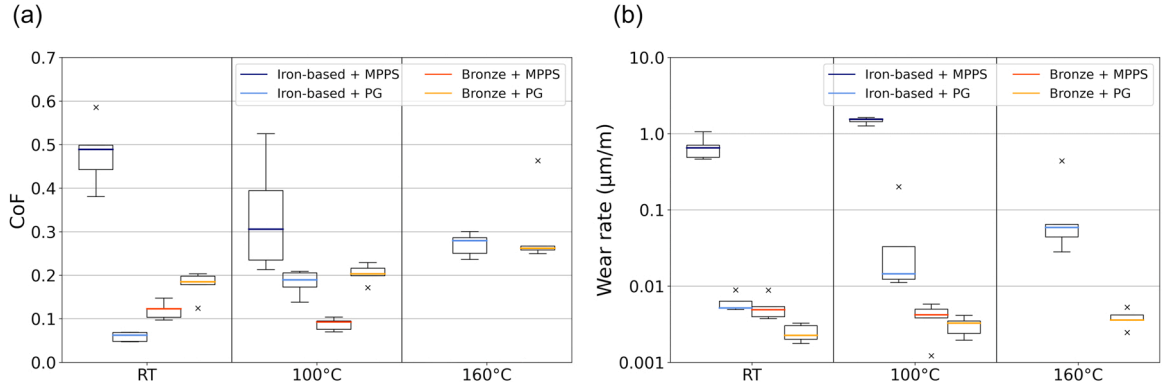

Fig. 5. (a) Coefficient of friction (CoF) box plot for iron-based and bronze bearings for different temperatures and lubricants. (b) Wear rate (wear/tested distance) box plot for iron-based and bronze bearings at different temperatures and lubricants. Wear rate in logarithmic scale. Each box represents the results of 5 parallel tests at the specified experimental parameters.

critical operation based on accelerometer data. In the following, the results of iron-based PJB + PG tests at 160°C are discussed, since the power spectral density map for this material combination exhibited the most pronounced features. Fig. 7 shows the JTFA of the accelerometer signal from position 1. In Fig. 7a, the temporal evolution of the accelerometer signal is presented together with the unprocessed motor torque signal. The graph displays the maxima of each HR window and exhibits significant increases at the beginning and end of the test. Fig. 7b shows an overview spectrogram of the test. For each HR window, one Fast Fourier Transform (FFT) spectrum was calculated. The individual FFT spectra are displayed color-coded in the form of vertical columns centered around the corresponding acquisition times. One can clearly distinguish three operation regimes: the steady state is preceded by an extended run-in phase, which lasted for 14 hours in the present test. Bearing failure was preceded by a distinctive critical operation phase starting 8 hours prior. Detail spectrograms of the three operation regimes are shown in Fig. 7c, together with graphs of the raw HR signals of the motor torque and the accelerometer from the corresponding time windows.

As already mentioned, the iron-based PJB material showed distinctive run-in characteristics. In the run-in phase, the motor torque signal (and hence the CoF) increased by about 30% at low rotation speeds. These increases were accompanied by massive spikes in the accelerometer signal, reaching values up to 3 g. This implies an increased contact between asperities at low speeds. During deceleration, this leads to the excitation of vibrations. A second, much less pronounced outburst in the accelerometer data occurs, when the journal starts rotating in the opposite direction, having to overcome static friction to change from stick to slip.

When the system reaches steady operation, the torque signal takes on a more rectangular shape, and the regular outbursts in the accelerometer signal vanish. Towards the end of the test, vibrations are induced at each direction change, implying a deterioration of the lubrication state and increased contact between asperities at low speeds. These outbursts in the accelerometer signal were asymmetric, more pronounced when the journal was moving in counterclockwise direction. This goes hand in hand with increased friction, visible in the increased torque signal.

As stated in Section 3.1, the CoF increase of the bronze bearings before failure was slower and much less severe compared to the iron-based PJB material. Also, no clearly defined run-in behavior was observed. These findings were also reflected in the accelerometer data. Fig. 8 shows JTFA results from one bronze bearing with MPPS lubricant at 100°C with a total lifetime of ≃ 80 h.

The severe outbursts observed in the accelerometer data of the iron-based PJBs are absent for the bronze material, with maxima of the accelerometer signal reaching only 0.2 g before failure. Nevertheless, a clear distinction between steady and critical operation can be obtained using JTFA.

In all tests, strong frequency contributions were observed below 0.5 kHz. These are connected to eigenfrequencies of the test rig itself and observable throughout the experiment. During run-in as well as towards the end of the test, a frequency contribution at approximately 0.12 kHz was observed. This frequency was numerically verified to be an eigenfrequency of the pendulum at the respective test position. The PSD of

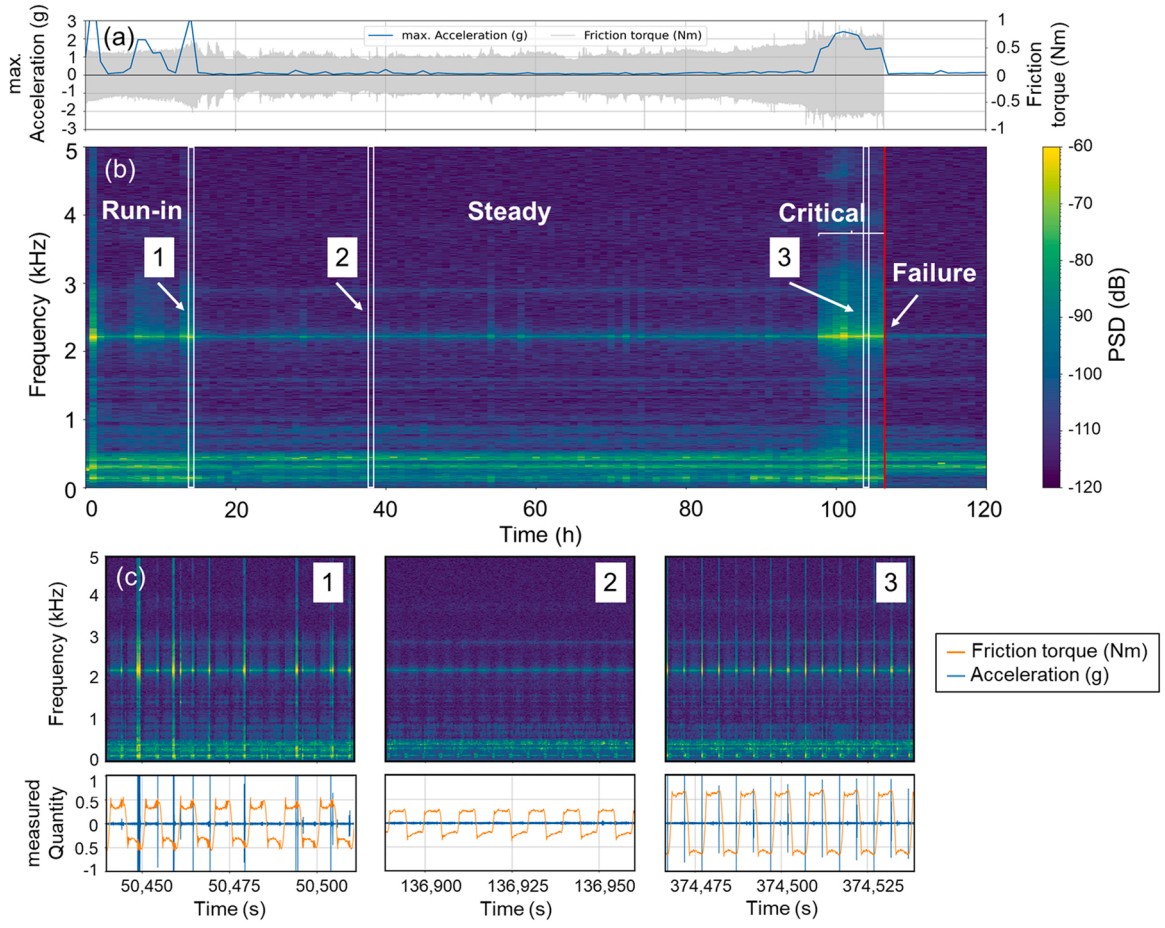

Fig. 7. JTFA of accelerometer data from one test position (iron-based PJB material, PG, 160°C). (a) Temporal evolution of accelerometer and unprocessed motor torque signals. Maximum acceleration values of HR windows are displayed. (b) Overview spectrogram of accelerometer signal. FFT spectra of HR windows are represented as vertical columns centered around the respective acquisition time. (c) Detail spectrograms of HR windows taken during run-in, steady, and critical operation. The graphs below represent the corresponding raw HR signals of the motor torque and the accelerometer.

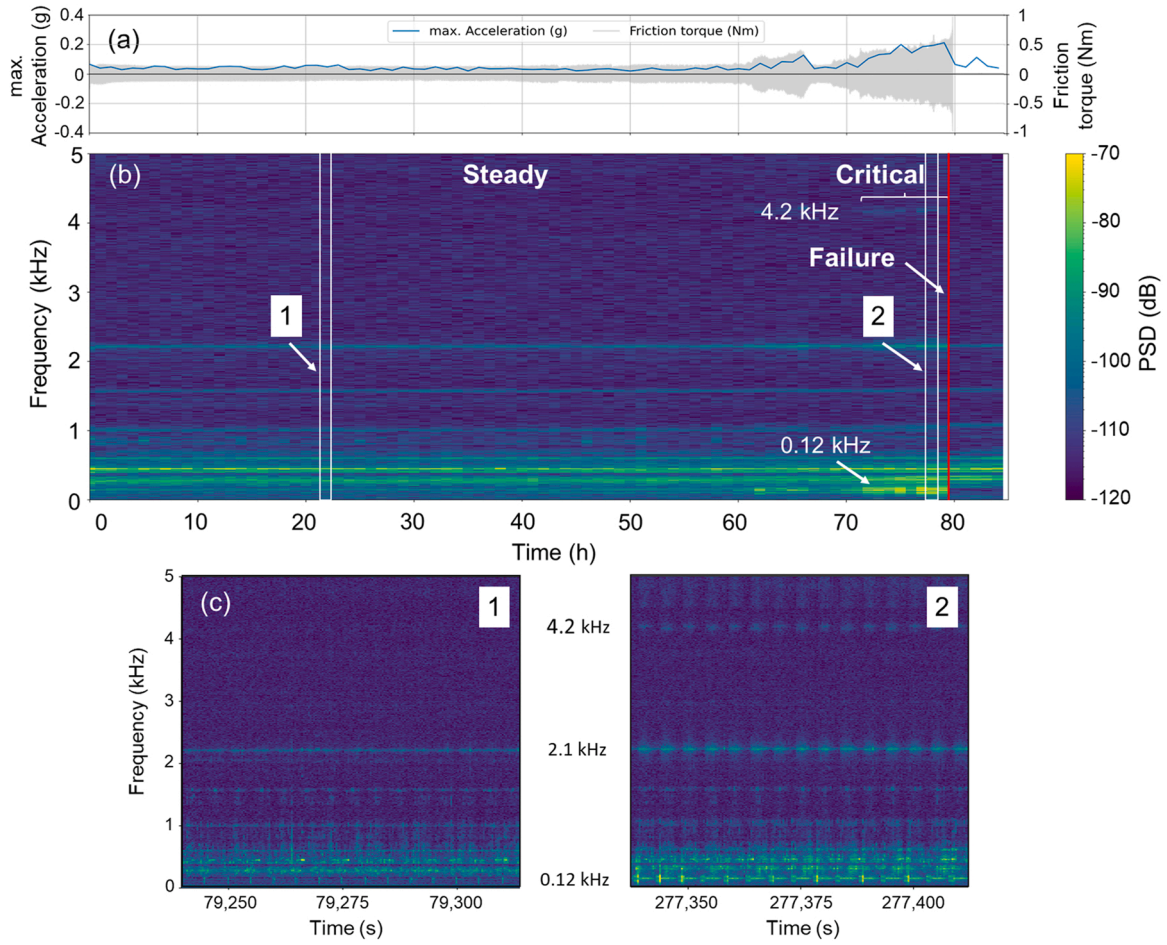

Fig. 8. JTFA of accelerometer data from one test position (bronze, MPPS, 100°C). (a) Temporal evolution of accelerometer and unprocessed motor torque signals. Maximum acceleration values of HR windows are displayed. (b) Overview spectrogram of accelerometer data. FFT spectra of HR windows are represented as vertical columns centered around the respective acquisition time. (c) Detail spectrograms of HR windows taken during steady and critical operation.

this frequency increases gradually, when the system reaches the end of its lifetime due to increased friction.

A frequency contribution at 2.1 kHz was observed in all tests and strongly intensified during run-in and critical operation. The intensity of the 2.1 kHz line is highest when the shaft reaches its highest speed and nearly vanishes at the turning points, thus creating a periodic, "pulsating" pattern in the spectrogram. These observations are clearly visible in the case of the iron-based PJBs (Fig. 7) and less pronounced for the bronze bearings (Fig. 8). In the latter case, an excitation of the second harmonic of this frequency (4.2 kHz) was observed when the system reached critical operation. Turning points are observable at low frequencies (< 0.5 kHz) throughout the test, producing a regular pattern in the spectrogram.

In general, the observed frequencies lie well above the applied rotation frequencies and are most likely caused by broadband excitation due to the stochastic nature of the solid contact between individual asperities. Note, however, that this paper does not aim at the detailed analysis of every contribution to the vibration signal's frequency components, but rather uses the obtained spectrogram to identify states of operation and the transitions in-between.

3.3. Lifetime of PJBs

The lifetimes of the bearing–lubricant combinations are summarized in Table 3. If the bearings did not fail during the testing period, its length is given following a greater-than sign, which implies that the only statement that can be made is that the bearing systems all operated longer than that duration. The integers in parentheses give the number of bearing systems that failed.

Table 3
Average lifetime (in h) and standard deviations for the different material, lubrication, and temperature conditions. Five bearing systems were tested per parameter combination. Values in parentheses indicate the number of failures for the respective test condition.

	RT	100°C	160°C
Iron + PG	> 282.8 (0)	> 334.4 (0)	122.9 ± 3.0 (3 + 2)[a]
Iron + MPPS	96.3 ± 13.0 (4)	2.5 ± 0.2 (5)	–
Bronze + PG	> 263.9 (0)	> 305.7 (0)	271.6 ± 12.7 (3)
Bronze + MPPS	> 284.6 (1)	102.0 ± 7.3 (4)	–

[a] Two bearings were close to failure when the experiment was stopped.

The survival probability P_{survival} of a bearing system as a function of the running time t can then be given in the form of a cumulative Weibull distribution function

$$P_{\text{survival}}(t;k,\lambda) = 1 - e^{-(t/\lambda)^k} \quad , \tag{6}$$

where k is the shape parameter and λ is the scale parameter of the Weibull distribution. We employed the median rank method to fit k and λ based on the time-to-failure data. This is done by ordering the times-to-failure t_{fail} for a given system in ascending order and assigning them ranks i running from 1 to n. The median ranks R_i are then obtained via the expression $R_i = (i - 0.3)/(n + 0.4)$. We can then plot $\ln[\ln(1/(1-R_i))]$ over $\ln(t_{\text{fail}})$ and perform a linear regression. The slope

of the resulting straight line $y = kx + d$ is the shape parameter k of the Weibull distribution, and the scale parameter $\lambda = \exp(|d/k|)$.

A value of $k < 1$ corresponds to a failure rate decreasing over time, which is a sign of high "infant mortality", while for $k = 1$, the failure rate does not change over time. Conversely, $k > 1$ means that the failure rate increases over time, a behavior that can be associated with a process of aging, making systems more likely to fail as time progresses.

We have plotted the survival probability for all those systems with sufficient data to allow a fitting in Fig. 9. The combination Iron + MPPS has a shape parameter smaller than 1 independently of the temperature, leading to an immediate onset of decay in the survival probability, i.e., having pronounced "infant mortality", while the other systems all have $k > 1$, which leads to well-defined running behavior and lifetimes.

3.4. Discussion

In the work presented here a combination of conventional tribometer data and high-rate accelerometer data was utilized to analyze and understand the evolution of the tribosystem "porous journal bearing". Both, the progress of friction and the probability of failure are studied in detail, giving insight in the current state of the tribosystem. This includes changes of power consumption due to frictional losses over time and characteristic changes of the acceleration patterns indicating impending failure, marking the necessity of maintenance actions.

The presented tool set, in particular the JTFA, can be adapted to long-term tests of any tribosystem, provided that a sensor capable of capturing the relevant frequency range can be installed. In our case, this was an accelerometer with a bandwidth of 20 kHz, whereby the subsequent data analyses revealed that the relevant information was entirely contained within the range 0–5 kHz. Accelerometer data were not acquired continuously, but only in bursts of 180 s at defined times. This means that the volume of the generated data may be reasonably handled using consumer-grade computer hardware. Furthermore, the tool set presented here is very well suited for online data analysis. Recorded data can be processed in real time and therefore the amount of stored data may be reduced significantly.

The real-time processing capability allows the development of algorithms to detect impending failures in real time. For example, in our case, the accelerometer data indicated a change in the operational state significantly before other quantities such as the motor torque exceed their preset critical threshold. Thus, applying such an algorithm in a real machine makes it possible to take timely countermeasures, such as adding lubricant on demand, exchange or repair of a component at the next scheduled time interval or, in the worst case, an emergency shutdown of the machine. Therefore, the presented work can be an important contribution to a predictive maintenance strategy. In addition, JTFA spectral data are very well suited to train a machine learning algorithm to classify patterns associated with critical system behavior [42] and to predict impending failure.

In addition to this early warning possibility via JTFA, a sufficient data source of "failed" bearings can be used to calculate the failure probability of a given system. The presented test rig allows for the parallel collection of such data in a significant amount at an accelerated testing time. With the help of Weibull plots, see Fig. 9, it is possible to derive the expected lifetime for a given material–lubricant pairing at given loading conditions.

The combination of JTFA on sensor data and lifetime analysis based on bearing failure permits to establish a robust workflow for improving not only bearing design but also maintenance strategy.

4. Conclusions

To setup a toolbox for efficiently monitoring the health status of tribosystems and generate data for lifetime predictions the use case porous journal bearing was utilized. A custom-built multiple bearing wear test rig with heatable sample support, allowing five simultaneous tests at increased aging rate, was used. Two different porous journal bearing materials and two different lubricants were studied at three test temperatures.

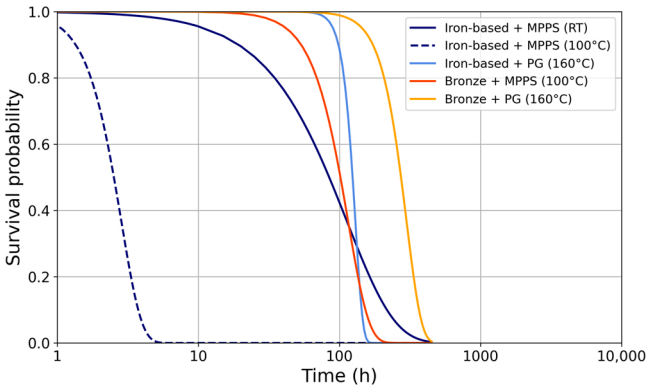

Fig. 9. Survival probability curves for all bearing systems with enough available data to allow fitting to a Weibull distribution. The actual numbers of failed bearings contributing to each curve are given in parentheses in Table 3.

As main feature, joint time-frequency analysis was applied to accelerometer data for ex-post evaluation of changes in the tribosystem over time. From a visual inspection of the power spectral density, we could make a clear distinction between the operational states from running-in to failure. In particular, the eigenfrequencies are amplified, while the noise level rises considerably during the run-in and critical states.

From the obtained times-to-failure, a lifetime assessment was formulated based on Weibull statistics. In addition to being able to accurately calculate an average service life, this approach also allows a qualitative characterization of the failure behavior, i.e., a clear disambiguation between high "infant mortality" and well-defined bearing operation.

In a further step, the presented tool set may form the basis of a monitoring system for the real-time assessment of the current "health state" of tribosystems in general, aid maintenance and will allow targeted optimization of material–lubricant combinations for specific applications. Combining joint time-frequency analysis with an appropriate machine learning algorithm will enable the classification of critical signal patterns in real-time as well as the early prediction of impending failure.

CRediT authorship contribution statement

J. Prost: Conceptualization, Data curation, Formal analysis, Investigation, Methodology, Software, Writing – original draft. **G. Boidi**: Conceptualization, Investigation, Methodology, Writing – original draft. **M. Varga**: Conceptualization, Writing – original draft. **G. Vorlaufer**: Conceptualization, Methodology, Supervision, Writing – original draft. **S.J. Eder**: Conceptualization, Investigation, Formal analysis, Writing – original draft.

Declaration of Competing Interest

The authors declare that they have no known competing financial interests or personal relationships that could have appeared to influence the work reported in this paper.

Acknowledgment

This work was funded by the Austrian COMET-Program (Project K2 InTribology1, no. 872176) and carried out at the Austrian Excellence Center for Tribology. The authors wish to thank Christoph Haslehner and Bettina Ronai for preparing the samples and running the tests. The

authors acknowledge TU Wien Bibliothek for financial support through its Open Access Funding Programme.

References

[1] Meurisse M-H. Porous Metal Journal Bearings. US, Boston, MA: Springer; 2013. p. 2669–73.
[2] Morgan VT, Cameron A. Mechanism of lubrication in porous metal bearings. Proc Conf Lubr Wear 1957:151–75.
[3] Braun AL. Porous bearings. Tribol Int 1982;15(5):235–42.
[4] Neacşu IA, Scheichl B, Vorlaufer G, Eder SJ, Franek F, Ramonat L. Experimental validation of the simulated steady-state behavior of porous journal bearings. J Tribology 2016;138(3):031703.
[5] Shi F, Wang QJ. A mixed-TEHD model for journal-bearing conformal contacts–part I: model formulation and approximation of heat transfer considering asperity contact. J Tribology 1998;120(2):198–205.
[6] Wang QJ, Shi F, Lee SC. A mixed-TEHD model for journal-bearing conformal contact–part II: contact, film thickness, and performance analyses. J Tribology 1998;120(2):206–13.
[7] Raman R, VinodBabu L. Tests on sintered bearings with reduced oil contents. Wear 1984;95(3):263–9.
[8] Sharma N, Kango S, Sharma RK, Sunil. Investigations on the effects of surface texture on the performance of a porous journal bearing operating with couple stress fluids. Int J Surf Sci Eng 2014;8(4):392–407.
[9] Amann T, Kailer A, Beyer-Faiß S, Stehr W, Metzger B. Development of sintered bearings with minimal friction losses and maximum life time using infiltrated liquid crystalline lubricants. Tribology Int 2016;98:282–91.
[10] Trachsel M, Pittini R, Dual J. Evaluation and quantification of friction using ionic liquids in small, self lubricating journal bearings. Tribology Int 2018;122:15–22.
[11] Eder SJ, Bianchi D, Neacşu IA, Vorlaufer G. An experimental and signal analysis workflow for detecting cold-induced noise emissions (cold squealing) from porous journal bearings. Mech Syst Signal Process 2019;115:60–9.
[12] Cameron A, Morgan VT, Stainsby AE. Critical conditions for hydrodynamic lubrication of porous metal bearings. Proc Inst Mech Eng 1962;176(28):761–70.
[13] Eder SJ, Ielchici C, Krenn S, Brandtner D. An experimental framework for determining wear in porous journal bearings operated in the mixed lubrication regime. Tribology Int 2018;123:1–9.
[14] Ielchici CD, Krenn S, Eder SJ. A tribometer and methodology for wear and friction testing of porous journal bearings at elevated temperatures. Ind Lubr Tribology 2020;72(8):1027–31.
[15] Boidi G, Krenn S, Eder SJ. Identification of a Material-Lubricant Pairing and Operating Conditions That Lead to the Failure of Porous. J Bear Syst Tribology Lett 2020;68(4).
[16] Cohen L. Time-frequency distributions - a review. Proc IEEE 1989;77(7):941–81.
[17] Daubechies I. The wavelet transform, time-frequency localization and signal analysis. IEEE Trans Inf Theory 1990;36(5):961–1005.
[18] Manhertz G, Bereczky As. Stft spectrogram based hybrid evaluation method for rotating machine transient vibration analysis. Mech Syst Signal Process 2021;154:112–7.
[19] Sun J, Wang R, Duan H-F. Multiple-fault detection in water pipelines using transient-based time-frequency analysis. J Hydroinform 2016;18(6):975–89.
[20] Chen X, Wang S, Qiao B, Chen Q. Basic research on machinery fault diagnostics: Past, present, and future trends. Front Mech Eng 2018;13(2):264–91.
[21] Sun R, Yang Z, Chen X, Tan Sa, Xie Y. Gear fault diagnosis based on the structured sparsity time-frequency analysis. Mech Syst Signal Process 2018;102:346–63.
[22] Jáuregui JC, Reséndiz JR, Thenozhi S, Szalay Tr, Jacsó Á, Takács M. Frequency and time-frequency analysis of cutting force and vibration signals for tool condition monitoring. IEEE Access 2018;6:6400–10.
[23] Lopes WN, Junior POC, Aguiar R, Alexandre FA, Dotto FRL, Da Silva PS, et al. An efficient short-time fourier transform algorithm for grinding wheel condition monitoring through acoustic emission. Int J Adv Manuf Technol 2021;113:585–603.
[24] Baccar D, Söffker D. Wear detection by means of wavelet-based acoustic emission analysis. Mech Syst Signal Process 2015;60–61:198–207.
[25] Rastegaev I, Merson D, Rastegaeva I, Vinogradov A. A time-frequency based approach for acoustic emission assessment of sliding wear. Lubricants 2020;8:52.
[26] Saeidi F, Shevchik SA, Wasmer K. Automatic detection of scuffing using acoustic emission. Tribology Int 2016;94:112–7.
[27] Shevchik SA, Saeidi F, Meylan B, Wasmer K. Prediction of failure in lubricated surfaces using acoustic time-frequency features and radnom forest algorithm. IEEE Trans Ind Inform 2017;13(4):1541–53.
[28] Ma J, Zhang H, Lou S, Chu F, Shi Z, Gu F, et al. Analytical and experimental investigation of vibration characteristics induced by tribofilm-asperity interactions in hydrodynamic journal bearings. Mech Syst Signal Process 2021;150:107227.
[29] Zhang H, Ma J, Li X, Xiao S, Gu F, Ball A. Fluid-asperity interaction induced random vibration of hydrodynamic journal bearings towards early fault diagnosis of abrasive wear. Tribology Int 2021;160:107028.
[30] Prost J, Boidi G, Lebersorger T, Varga M, Vorlaufer G. Comprehensive review of tribometer dynamics - cycle-based data analysis and visualization. Friction 2021.
[31] G. Boidi, IS Tertuliano, MF Cano, GAA Machado, RM Souza, and IF Machado. Tribological evaluation of sintered and conventional gear materials. Technical report, SAE Technical Paper, 2017.
[32] Boidi G, Tertuliano IS, Lima LGBS, Profito FJ, Machado IF. Porosity effect of sintered steel on the frictional performance of conformal and nonconformal lubricated contacts. Tribology Trans 2019;62(6):1029–40.
[33] Ebner M, Omasta M, Lohner T, Sperka P, Krupka I, Hartl M, et al. Local Effects in EHL Contacts with Oil-Impregnated Sintered Materials. Lubricants 2019;7(1):1.
[34] Rasband S, et al. ImageJ 1997.
[35] Detter H. A study of the operating behavior of precision pivot bearings. Wear 1973;26(1):121–32.
[36] N. Hiraoka.On the Friction of Oil-Impregnated Sintered Bearings, chapter 2. IntechOpen, 2019.
[37] OSIMESS Two-point measuring system for bores from ø1,0 mm, 2021.⟨http://www.schwenk-lmt.de/61pv45zz.pdf⟩.
[38] Vio R, Wamsteker W. Joint time-frequency analysis: A tool for exploratory analysis and filtering of non-stationary time series. Astron Astrophys 2002;388(3):1124–38.
[39] Harris FJ. On the use of windows for harmonic analysis with the discrete fourier transform. Proc IEEE 1978;66(1):51–83.
[40] Boidi G, Fukumasu NK, Machado IF. Wear and friction performance under lubricated reciprocating tests of steel powder mixtures sintered by spark plasma sintering. Tribol Int 2018;121:139–47.
[41] Fukumasu NK, Boidi G, Seriacopi V, Machado GAA, Souza RM, Machado IF. Numerical analyses of stress induced damage during a reciprocating lubricated test of fecmo sps sintered alloy. Tribol Int 2017;113:443–7. 43rd Leeds - Lyon Symposium on Tribology 2016.
[42] Pandiyan V, Prost J, Vorlaufer G, Varga M, Wasmer K. Identification of abnormal tribological regimes using a microphone and semi-supervised machine-learning algorithm. Friction 2021;94.